Nonintrusive Arrhythmia Detection from Wrist Pulse Using NTSC Color Model in Eulerian Video Magnification

Baby Lolita Basyah[1], Hustinawaty[2], Miftahul Jannah[3,*]

[1,2,3]*Department of Information Systems, Gunadarma University, Depok, 16451, Indonesia*

(Received: November 20, 2025; Revised: January 25, 2026; Accepted: April 8, 2026; Available online: May 3, 2026)

Abstract

Arrhythmia is a cardiovascular condition characterized by abnormal heart rhythms, such as tachycardia and bradycardia, which may lead to serious health complications if not detected early. This study proposes a non-invasive approach for screening tachycardia by extracting pulse signals from wrist video recordings using Eulerian Video Magnification (EVM) combined with the NTSC color space model. Subtle variations in skin color caused by blood flow, which are typically imperceptible to the human eye, are amplified using the EVM technique to enhance pulse-related motion signals. The NTSC color model is employed to separate luminance and chrominance components (YIQ), allowing more effective identification of pulse-induced color variations in the wrist region. The recorded wrist videos are processed through several stages, including spatial decomposition, temporal filtering, motion magnification, and pixel intensity extraction from the region of interest to obtain a temporal pulse signal. Peak detection is then applied to estimate heart rate in beats per minute (BPM). The performance of the proposed method is evaluated by comparing the estimated BPM values with reference measurements obtained from a Xiaomi Mi Band 2 wearable device. Experimental results based on 20 wrist video recordings demonstrate that the proposed method achieves approximately 96% agreement between the estimated BPM values and the reference measurements. Quantitative evaluation using Mean Absolute Error (MAE), Root Mean Square Error (RMSE), and correlation analysis further confirms the consistency of the proposed approach. These results indicate that the integration of Eulerian Video Magnification with the NTSC color model has potential as a low-cost and non-contact method for preliminary tachycardia screening and remote cardiovascular monitoring.

Keywords: Arrhythmias, Pulse, Blood Flow Velocity, Heart, Video Recording

1. Introduction

Arrhythmia is caused by special cells in the heart that generate electrical potential which experience obstacles in the propagation of the signal, which has an effect on heart rate that becomes abnormal. Heart rate is one of the indicators of human health that is most often measured [1], defined as the number of times the heart beats per minute. A healthy adult human usually has a normal heart rate at rest between 60-100 beats per minute [2]. To get the right measurements in heart rate measurement technology, at this time most physical contact with patients is still needed. Direct contact between ECG electrodes and the patient's skin can cause dermatological reactions such as redness, itching, and irritation, particularly in individuals with a history of skin allergies. These reactions are often due to allergens or irritants present in the electrodes or conductive gels used during ECG monitoring [3].

Important information about a person's health that is reflected by pathological changes can be obtained from wrist pulse signals. Experiments show that there is a high correlation between the shape of the wrist pulse signal and the variation in blood volume [4], [5]. The human visual system has limited sensitivity to spatio-temporal signals, hence many of them cannot be detected. For example, human skin color varies slightly with blood flow. This variation which is not visible to the eye can be captured to detect the pulse [6], [7]. Other study had utilized the EVM method to reveal the value of pixel color changes within a certain set of time in each space and amplifying variations in the desired temporal frequency but not yet using the NTSC color space [8], [9].

In this study, we aimed to overcome the difficulty in tachycardia screening nonintrusively by extracting pulses and enlarge image of the human wrist using the NTSC color space model in the EVM method. This study represents an

***Corresponding author: Miftahul Jannah (miftah@staff.gunadarma.ac.id)**
DOI: https://doi.org/10.47738/jads.v7i2.1293

ISSN 2723-6471

initial step focusing on tachycardia as the form of arrhythmia most clearly detected through rapid heart rate variations. Further development is needed to include other types of arrhythmias such as bradycardia, atrial fibrillation, and premature ventricular contractions. With this detection of noncontact results that vary due to human error can be minimized and sufficient to do on the wrist, because this position is the position that is most easily found and acquired in the human body. The steps taken consisted of wrist video acquisition using a mobile camera, changing the color space from RGB to NTSC, decomposing the image into several sizes using the Laplacian pyramid, filtering using IIR, magnification of the image using Euler Magnification, and reconstruction to restore the image into its original form as before decomposition. The peak was found with the peak detection algorithm, then the signal frequency is calculated from the location of the peak and the pulse is obtained. The results of the heart rate were compared with the actual heart rate measured using the Xiaomi Mi Band 2 device which has a heart rate sensor [10] to validate the heart rate accurately and the final step was to tachycardia screening based on the pulse rate obtained.

2. Literature Review

Several studies related to arrhythmias and heart rate detection had already been conducted. A study on contactless heart rate measurement on the chest surface used a grid-based stereoactive method as an alternative to ECG measurements. however, arrhythmia detection was not performed and respiratory motion affected the accuracy of the measurements [11]. Another study used Kinect as a motion sensing device to detect heart rate by analyzing skin color changes caused by blood flow [12]. Recent developments have also demonstrated that camera-based physiological monitoring can estimate heart rate from subtle color and motion variations captured in video sequences [13], [14].

Research on heart rate monitoring from the face and hand using an Xbox 360 camera has been conducted [15] however, arrhythmia detection was not included, and accurate face detection remains a challenge. Recent studies further improved the robustness of video-based heart rate monitoring under different lighting conditions and subject movements [16], [17].

Heart rate estimation using video depth tracking to detect heartbeat at the tip of the nose using Gaussian Markov Random Fields (GMRF) and Fast Fourier Transform (FFT) has also been proposed [18]. However, arrhythmia identification was not addressed in this approach. Other studies detected arrhythmia using photodiodes and infrared LEDs, processed by Arduino Uno [19]. However, this system requires direct contact with the skin. Pansare measured heart rate from the face and wrist using video zooming techniques, but arrhythmia detection and NTSC color space processing were not included [20]. Most existing studies have not addressed arrhythmia detection using a contactless wrist-based approach with optimized color space processing. However, several recent studies highlight the growing interest in remote photoplethysmography and video-based vital signs monitoring for healthcare applications [21], [22].

3. Methodology

Research to indicate arrhythmias by detecting pulses on the wrist includes four main stages that describes how a video is captured by a camera which is then processed to show the movement of a person's pulse. The first stage is the wrist video acquisition process, the second stage is the process of enlarging the movement with the Eulerian Magnification Method and the third stage is pulse frequency extraction, the fourth stage arrhythmias identification. The following figure 1 is a general description of processes.

ISSN 2723-6471

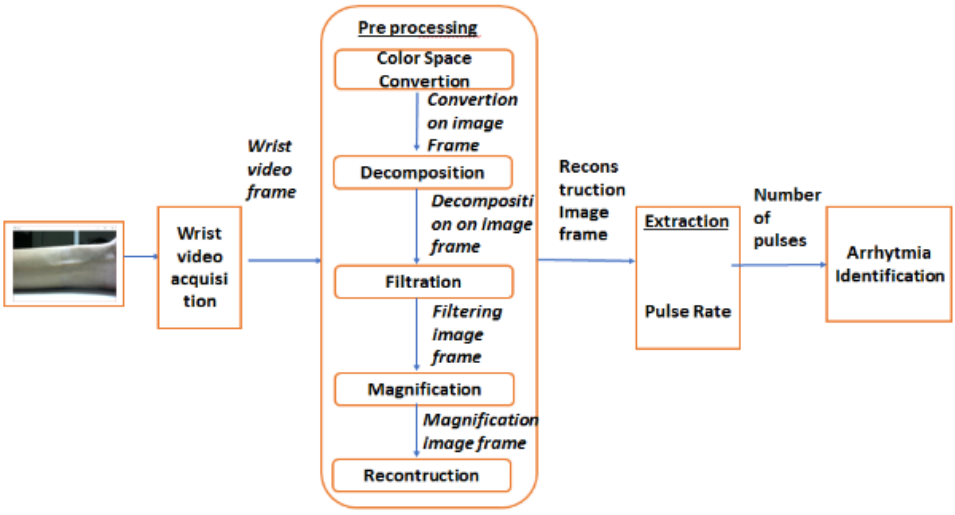

Figure 1. Research framework for nonintrusive identification of arrhythmia in human wrist pulse rate based on heart rate frequency using NTSC color space models on Eulerian Video Magnification

3.1.Video Acquisition

Human wrist video recording can be done in real-time in a resting or non-resting state [23], [24]. The room used is ensured to have consistent lighting conditions during the video recording process of at least 500 Lux and a camera resolution of 12MP + 5MP to produce good wrist videos. During recording, the position of the cellphone camera is directly in front of the wrist object at a distance of 10-15 cm and the camera height is parallel to the wrist. Video recordings with a duration of 6 seconds are saved with a resolution of 1280 x 720 pixels. The following is Algorithm 1 for the video acquisition stage.

Algorithm 1. Acquisition of Wrist Video

Input: wrist object

1. Camera calibration process
2. Camera initialization
3. Create a storage folder
4. Determine ROI
5. Recording wrist objects

Output: RGB image

For initialization phase, the smarphone's camera is connected to the laptop using the DroidCam application, allowing the system to recognize the phone's camera as a webcam on the laptop. After the initialization process is complete, a folder is created to store the recorded videos. The folder name uses the date-month-year format, along with the hour-minute-second date to indicate the start time of the recording process. Next, the video recording process begins by capturing images frame by frame, which are then saved in .jpg format. Once the number of frames reaches 162, equivalent to a 6 second video at 27 fps, all frames are combined and saved as a .mp4 video in the created folder. The second stage of the process is enlarging the movement with Eulerian Magnification Method. The general description of the EVM method is shown in figure 2.

The wrist video that has been acquired, is then opened and frame-by-frame image reading process is carried out, then be converted into the NTSC model, decomposed using the Laplace Pyramid so that changes in the edge are obtained. After that the image frame undergoes a temporal filtering process to filter the frequency so that later it will make the image easy to observe. Then the image frame magnification process is carried out to get an enlargement of the movement of the pulses so that they are visible to the eye. Then the reconstruction process of the decomposed image frame is carried out. The image frame is then saved in the *.jpg format. If all frames have been processed, the magnified video is saved in the provided folder

ISSN 2723-6471

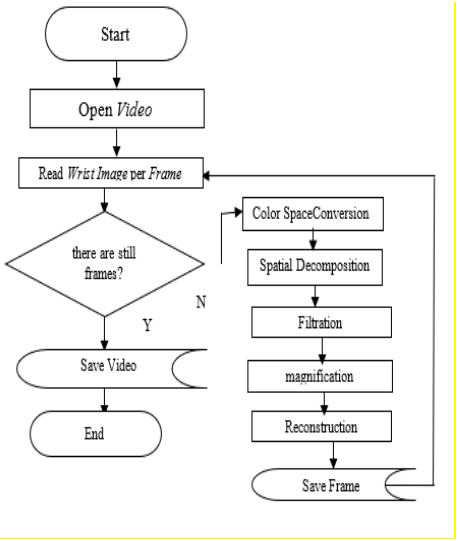

Figure 2. General description of the Eulerian Magnification process

3.2. Color Space Conversion

Initially the acquired wrist image is a color image with RGB color space, for the sake of visual interpretation the color space is changed to NTSC / YIQ. The main information of the image is in its luminous components and the human eye is very sensitive to changes in luminance rather than chrome changes. Changing the color space is done to clarify the magnification that occurs in the movement of the pulse at the time of the magnification that requires sufficient lighting to make certain aspects of the image more clearly visible [25]. Algorithm 2 is an algorithm for converting RGB to NTSC color space.

Algorithm 2. Convert RGB Image to NTSC Color Space

Input: RGB image

1. Read the RGB image
2. Y = 0.299R + 0.587G + 0.114B
3. I = 0.595716R – 0.274453G – 0.321263B
4. Q = 0.211456R – 0.522591G + 0.311135B

Output: NTSC image

3.3. Decomposition

The image is decomposed using Laplacian Pyramid. This decomposition aims to find edges in the image and decompose the image into several sizes and multilevel. In this study five levels of decomposition of the image are used, each of which has a different level of sharpness.

The image at Laplacian Pyramid level is obtained based on the reduction of the image at Gaussian Pyramid with the same level reduced by the image at the next level of Gaussian Pyramid which has been expanded according to the size at the i level. Algorithm 3 is an algorithm for the process of decomposition of images into several sizes and levels using Laplacian Pyramid.

Algorithm 3: Image Decomposition

Input: Image

1. current img ← NTSC image
2. I ← 1
3. If I > 5, the process ends
4. Gaussian (i) ← current img
5. Mat Up = Gaussian (i)

ISSN 2723-6471

6. Resize curr img
7. Save in Mat Down
8. current Img ← Mat Down
9. Lap (i) ← Mat Up - Mat Down
10. i = i + 1; go back to step 3

Output: decomposed image / laplace pyramid

3.4. Filtration

The process of filtering the wrist image is done with the aim of removing the frequency at the image that is too low which can make changes in the image difficult to observe. Besides filtering also aims to remove high frequencies in the image to eliminate the noise contained in the image which causes the image difficult to be observed.

This research uses a type of filtering that works in real time with the aim to get good performance computationally so that the detection results will later work in real time. The filtering used in this study is IIR (Infinite Impulse Response) [26]. Two recursive low-pass filters are applied to the Laplacian pyramid coefficients extracted from each video frame to formally describe the temporal filtering process. Filtering is described in algorithm 4. In the formal temporal filtering process, two recursive low-pass filters are applied to the Laplacian pyramid coefficients extracted from each video frame.

$$LP_1(i) = (1 - fh)LP_1(i-1) + fh\ P(i) \quad (1)$$

$$LP_2(i) = (1 - fl)LP_2(i-1) + fl\ P(i) \quad (2)$$

The temporal bandpass signal is then obtained by subtracting the two filtered signals.

$$F(i) = LP_1(i) - LP_2(i) \quad (3)$$

P(i) represents the Laplacian pyramid coefficient at frame i, while fh and fl denote the filter coefficients controlling the response to higher and lower temporal variations. In this study, the coefficients are set to fh = 0.43 and fl=0.04 to suppress slow illumination changes and high-frequency noise while preserving the temporal variations associated with the wrist pulse signal.

Algorithm 4: Image Filtering

Input: decomposed / Laplace pyramid image

1. I ← 1
2. input vector the pyramid laplace per frame
3. If the frame runs out, the process ends
4. If the first frame initializes filtered = pyramid laplace;
   lowpass1 = vector pyramid laplace;
   lowpass2 = vector pyramid laplace;
   fh = 0.43; fl = 0.04
5. If it is not the first frame:
   Lowpass1 (i) = (1 - fh) * lowpass1 (i-1) + fh * pyrlap (i)
   Lowpass2 (i) = (1 - fl) * lowpass2 (i-1) + fl * pyrlap (i)
   Filtered (i) = lowpass1 (i) - lowpass2 (i)
6. i = i + 1
7. return to step 1

Output: filtered image

Human heart rate typically ranges between 60 - 100 beats per minute (BPM), which corresponds to a temporal frequency range of approximately 1–1.67 Hz. The temporal filtering stage aims to preserve signal variations within

 ISSN 2723-6471

this frequency range while suppressing unrelated temporal variations caused by illumination changes, motion artifacts, and other noise sources.

3.5. Magnification

Magnification can be defined as a process for magnification. Magnification aims to increase the amplitude of the image to obtain the magnification of the motion of an image, so that an image that originally had only a small amount of movement that is not visible to the eye will become visible to the eye. In this study the magnification carried out is the magnification of the movement of the pulses so that it is visible to the eye. To perform this magnification process, the EVM method is used. Algorithm 5 is an algorithm of magnification.

Algorithm 5. Image Magnification

Input: filtered image

1. level = 1; frame = 0
2. If frame > 1 and the frame runs out, the process ends
3. Input vector mat filtered per frame; width = filtered width; height = filtered height; Lamda_c = 80; alpha = 100; exaggeration_factor = 2.0
4. Lamda = sqrt (WidthxWidth + Height x Height);

   Delta = lamda_c / 8.0 / (1.0 + alpha); exaggeration_factor = 2.0; I = 0
5. If I < 5 do the loop to step 2
6. If I = 5 curlevel initialization = 1;

   curAlpha = lamda / delta / 8 - 1;

   curAlpha = curAlpha * exaggeration_factor
7. If curLevel = 5 or curLevel = 0 then dst = filtered (i) x 0;

   Besides that, then dst = src * min (alpha, curAlpha)
8. Calculate Lamda = Lamda / 2.0
9. Looping returns to step 5 for the next level

Output: image magnification

3.6. Reconstruction

Reconstruction is carried out on an image that has undergone a process of magnification, because the image has not returned to its original form, still in the form of the Laplace Pyramid. Therefore, the image needs to be reconstructed again from the image that has been spatially decomposed into a fully formed image. Algorithm 6 for image reconstruction to original form.

Algorithm 6. Reconstruction To Recombine Decomposed Images

Input: image magnification

1. Input currentImg = pyramid [level]
2. For i ← level - 1 to 0 step -1
3. Mat Up = currentImg
4. currentImg = Mat Up + pyramid [i]
5. Next i
6. Dst = currentImg

Output: the image that has fused back to its original shape

 ISSN 2723-6471

So that the image can be clearly seen by the eye after it is reconstructed to its original form, the color space of the image is returned to the RGB color space. The following Algorithm 7 is an algorithm for returning to the original RGB color space.

Algorithm 7. Convert NTSC Image to RGB Color Space

Input: NTSC image

1. Read the NTSC image
2. R = Y + 0.9563I + 0.6210Q
3. G = Y – 0.2721I – 0.6474Q
4. B = Y – 1.1070I + 1.7046Q

Output: RGB image

After separating the RGB components into the planes matrix, reconstruction is also carried out to reduce noise due to the magnification process. Algorithm 8 reduces noise due to magnification process.

Algorithm 8. Reconstruction to Reduce Noise Due to Magnification

Input: RGB image that has been reunited to its original form

1. Initialize the input matrix (src);

   output matrix (etc.);
2. The src matrix is then separated into the planes matrix array
3. Multiplying the color value in the plane matrix with the chromAttenuation value (0.1) to reduce noise due to the magnification process
4. Then the plane matrix is put back together and stored in variables dst

Output: image of reconstruction results

3.7. Pulse Rate Extraction

At the pulse extraction stage, pulse frequencies are obtained by counting the number of pulses per minute (BPM). figure 3 is a flowchart for calculating the pulse.

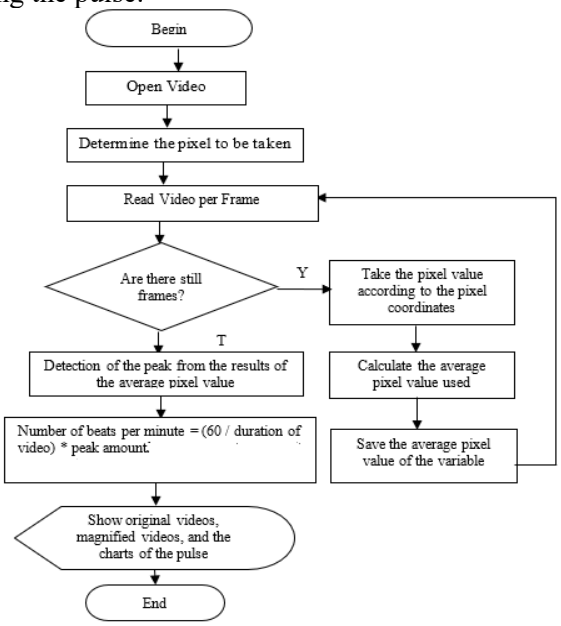

Figure 3. The flowchart for the pulse rate calculation process

To calculate the pulse rate, the magnified video is opened and then the pixels in the radial artery are determined so that the pixel values can be taken at the location of the pulse. The video is read frame-by-frame and each frame is converted to grayscale. The pixels that have been previously determined are taken their values, to be calculated their average values. The sequence of average pixel intensity values forms a temporal signal that reflects subtle variations in skin color caused by blood flow in the radial artery [27]. Similar approaches have been widely used in remote photoplethysmography for extracting cardiovascular signals from video recordings [28].

Before performing peak detection, the extracted pulse signal undergoes a preprocessing stage to reduce noise and improve signal stability. The Eulerian Video Magnification process enhances subtle color variations associated with blood flow while suppressing unrelated variations caused by lighting changes or minor movements. As a result, the periodic component of the pulse signal becomes more prominent, enabling clearer identification of heartbeat-related peaks in the temporal signal. After the temporal filtering process, peak detection is applied to this signal by identifying local maxima that correspond to individual pulse events. Each detected peak represents a heartbeat, and the total number of peaks within the observation period is then used to estimate the heart rate in beats per minute (BPM). The average values are stored in the variable y, then peak values are determined to be stored in the variable x. The heart rate is then calculated based on the number of detected peaks using Equation (4).

$$\text{BPM} = (60 \,/\, \text{T}) * \text{N} \tag{4}$$

where N represents the total number of detected pulse peaks and T denotes the duration of the video recording in seconds. The final step is to determine the pulse condition using the arrhythmia identification algorithm presented in Algorithm 9.

3.8. Identification of Arrhythmia

The first thing to do is reading the number of pulses per minute (BPM) obtained, then check whether the number of pulses per minute is less than 60, if so then the arrhythmia of Bradicardia is indicated. Then check whether the number of pulses per minute is more than 100, if so this indicates the symptoms of tachycardia arrhythmia. In addition to these conditions, for the number of pulses per minute 60 to 100 can be said to be indicated no bradycardia or tachycardia arrhythmia.

Algorithm 9. Arrhythmia Algorithm

Input: Number of pulses per minute (BPM)

1. If the pulse count is < 60 then the result = 'indicated arrhythmia of bradycardia'
2. If the pulse count is > 100 then the result = 'indicated tachycardia arrhythmia'
3. Else result = 'is not indicated bradycardia / tachycardia arrhythmia'
4. End

Output: Identification of arrhythmias

3.9. Performance Evaluation

This analysis emphasizes the comparison between the estimated BPM values and measurements from the wearable device using quantitative metrics consisting of correlation analysis, Mean Absolute Error (MAE), and Root Mean Square Error (RMSE). Mean Absolute Error (MAE) represents the average absolute difference between the estimated BPM values obtained by the proposed method and the reference BPM values obtained from the wearable device, as defined in Equation (5).

$$MAE = \frac{1}{N} \sum_{i=1}^{N} |X_I - X| \tag{5}$$

The Root Mean Square Error (RMSE) evaluates the magnitude of estimation errors while giving higher weight to larger deviations, as defined in Equation (6).

 ISSN 2723-6471

$$RMSE = \sqrt{\frac{1}{N}\sum_{i=1}^{N}(X_i - X)^2} \quad (6)$$

Additionally, the Pearson correlation coefficient (r) is used to measure the linear relationship between the estimated BPM and the reference BPM values.

$$r = \frac{\sum_{i=1}^{N}(X_i - \bar{X})(Y_i - \bar{Y})}{\sqrt{\sum_{i=1}^{N}(X_i - \bar{X})^2}\sqrt{\sum_{i=1}^{N}(Y_i - \bar{Y})^2}} \quad (7)$$

X_i represents the estimated BPM obtained from the proposed method, X (or Y_i) denotes the reference BPM measured using the wearable device, and N represents the total number of measurement samples used in the experiment.

4. Results and Discussion

In this study, heart rate data was collected from the wrist in real time using a smartphone camera, and the results were compared with the measurements obtained from the wearable device. The wearable device used in this experiment was the Xiaomi Mi Band 2, which has a built-in heart rate sensor. The wearable device was placed on the opposite wrist and operated simultaneously during the measurement process, as illustrated in figure 4.

Figure 4. Display of the results of pulse rate calculation

The experiment used 20 video recordings obtained from separate measurement sessions under resting conditions. Each recording represents a heart rate measurement taken from the wrist area and compared with a wearable device. The dataset was collected to evaluate the signal extraction performance of the proposed method without demographic attributes. The heart rate measurement results are presented in tables 1–3. The complete dataset used in this study is not fully presented.

The results for the low BPM category (<80) are presented in table 1. This table compares the BPM values estimated by the proposed method with reference measurements obtained from the used device. Only one sample fell into this category, indicating that low heart rate conditions were limited during the experiment.

Table 1. Pulse Calculation Test Results Low BPM (< 80)

Trial	Original Wrist Frame	Magnified Wrist Frame	Application (BPM)	Miband 2 (BPM)	Identification of Arrhythmia Application
1.			70	73	Not identified

ISSN 2723-6471

Results for the normal BPM category (80–100) are shown in table 2. There are 17 samples in this category, representing resting heart rate conditions. Comparisons between the proposed method and the reference wearable device within this normal heart rate range demonstrate consistency.

Table 2. Pulse Calculation Test Results Normal BPM (80 - 100)

Trial	Original Wrist Frame	Magnified Wrist Frame	Application (BPM)	Miband 2 (BPM)	Identification of Arrhythmia Application
1.			89	94	Not identified
2.			80	94	Not identified
3.			89	102	Not identified
4.			80	94	Not identified
5.			80	93	Not identified
6.			80	85	Not identified
7.			80	85	Not identified
8.			80	87	Not identified
9.			89	82	Not identified
10.			80	83	Not identified
11.			80	76	Not identified
12.			80	71	Not identified
13.			80	81	Not identified

ISSN 2723-6471

14.			80	83	Not identified
15.			89	86	Not identified
16.			89	90	Not identified
17.			89	89	Not identified

Results for the high BPM category (>100) are presented in table 3, containing two samples classified as tachycardia. This demonstrates the ability of the proposed method to estimate BPM values close to the reference measurements obtained from the device used.

Table 3. Pulse Calculation Test Results High BPM (> 100)

Trial	Original Wrist Frame	Magnified Wrist Frame	Application (BPM)	Miband 2 (BPM)	Identification of Arrhythmia Application
1.			104	102	Tachycardia was identified
2.			103	102	Tachycardia was identified

Based on 20 measurement samples, the MAE obtained was 5.65 BPM, RMSE was 7.22 BPM, correlation analysis yielded a coefficient of approximately 0.70, indicating a strong positive relationship between the estimated BPM values and the reference measurements obtained from the wearable device. Furthermore, the average BPM value obtained from the proposed method was 83.1 BPM, while the average BPM measured using the Xiaomi Mi Band 2 device was 86.55 BPM. Based on these results, the agreement between the two measurements reached approximately 96%. indicating that the estimated BPM values using the proposed video-based heart rate detection method were generally consistent with the values obtained from the reference wearable device.

Several factors contribute to discrepancies between estimated BPM values and reference measurements, including the time difference between video capture and sensor measurement, motion during recording, skin thickness, skin color, and the location of the pulse signal on the wrist. These factors can affect the clarity of color variations captured in video frames and impact the accuracy of BPM estimation. Unlike previous studies, which have largely focused on non-contact heart rate detection, this study extends the analysis by filtering tachycardia using the EVM method combined with the NTSC color model. This approach enhances pixel color variations associated with blood flow, thereby improving the visibility of heart rate-related changes in wrist video frames.

5. Conclusion

This paper presents the implementation of the NTSC color space model in the EVM to tachycardia screening in the video of the human wrist by enlarging the pulse movement so that the movement is more clearly visible. In this study, acquisition of video from the wrist can be performed, redisplaying the video from the acquisition and the video resulting from the Eulerian Magnification process accompanied by a graph of the visible pulses and the calculation of the pulse in units of beats per minute. In addition, each frame of the acquisition video and the magnification results will be stored in the original folder and magnification folder.

Based on the results of tests conducted, 20 data obtained from the trial results showed that 18 were detected as normal rates and 2 were detected as tachycardia arrhythmias, while the percentage of match between the results of the research with the results using the Mi Band 2 device was 96%. The difference in beats count results obtained is influenced by several factors, such as the difference in the time of video acquisition with the time of calculation on the Mi Band 2 device. In this research, the NTSC color space model in EVM can be used to further clarify small movements, so if there is movement during the video acquisition process will affect the results obtained. As well as factors such demographic variables such as age, gender, and skin tone were not recorded in this study, therefore their influence could not be quantitatively analyzed. The 96% value represents the agreement percentage between BPM estimated by the proposed method and BPM measured using the Xiaomi Mi Band 2 reference device. In the revised manuscript, evaluation metrics such as Mean Absolute Error (MAE), Root Mean Square Error (RMSE), and correlation analysis are added to clarify the calculation.

6. Declarations

6.1. Author Contributions

Conceptualization: B.L.B., H., and M.J.; Methodology: B.L.B., H.; Software: H., M.J.; Validation: B.L.B., H., and M.J.; Formal Analysis: B.L.B., H., and M.J.; Investigation: B.L.B., H.; Resources: B.L.B.; Data Curation: B.L.B., H.; Writing Original Draft Preparation: B.L.B., H., and M.J.; Writing Review and Editing: B.L.B., H., and M.J.; Visualization: M.J.; All authors have read and agreed to the published version of the manuscript.

6.2. Data Availability Statement

The data presented in this study are available on request from the corresponding author.

6.3. Funding

The authors received no financial support for the research, authorship, and/or publication of this article.

6.4. Institutional Review Board Statement

Not applicable.

6.5. Informed Consent Statement

Not applicable.

6.6. Declaration of Competing Interest

The authors declare that they have no known competing financial interests or personal relationships that could have appeared to influence the work reported in this paper.

References

[1] S. Srinivas, B. Vignesh R. K., V. N. Ayinapudi, A. Govindarajan, S. S. Sundaram, and N. Priyathersini, "Neurological consequences of cardiac arrhythmias: relationship between stroke, cognitive decline, and heart rhythm disorders," *Cureus,* vol. 16, no. 3, pp. 1–12, 2024, doi: 10.7759/cureus.57159.

[2] Y. Choi, G. Kim, J. Yoon, and Y. S. Kim, "Association of resting heart rate and physical activity with cardiovascular mortality: a population-based cohort study of Korean adults," *J. Sports Sci*., vol. 42, no. 16, pp. 1529–1537, 2024, doi: 10.1080/02640414.2024.2400807.

[3] C. C. Kellogg, A. W. Choi, and D. W. Shaw, "Allergic contact dermatitis to p-tert-butylphenol-formaldehyde resin from the label adhesive of an electrocardiogram electrode," *Dermatitis,* vol. 33, no. 1, pp. e2–e5, 2022, doi: 10.1097/DER.0000000000000838.

[4] C. Guo, Z. Jiang, H. He, Y. Liao, and D. Zhang, "Wrist pulse signal acquisition and analysis for disease diagnosis: a review," *Comput. Biol. Med.,* vol. 143, no. Apr., pp. 1–12, 2022, doi: 10.1016/j.compbiomed.2022.105312.

[5] B. Ibrahim and R. Jafari, "Cuffless blood pressure monitoring from an array of wrist bio-impedance sensors using subject-specific regression models: proof of concept," *IEEE Trans. Biomed. Circuits Syst*., vol. 13, no. 6, pp. 1723–1735, 2019, doi: 10.1109/TBCAS.2019.2956255.

[6] M. Cao, T. Burton, G. Saiko, and A. Douplik, "Remote photoplethysmography with a high-speed camera reveals temporal and amplitude differences between glabrous and non-glabrous skin," *Sensors*, vol. 23, no. 2, pp. 1–12, 2023, doi: 10.3390/s23020615.

[7] S. Premkumar and D. J. Hemanth, "Intelligent remote photoplethysmography-based methods for heart rate estimation from face videos: a survey," *Informatics*, vol. 9, no. 3, pp. 1–12, 2022, doi: 10.3390/informatics9030057.

[8] H. Lauridsen, S. Gonzales, D. Hedwig, K. L. Perrin, C. J. A. Williams, P. H. Wrege, M. F. Bertelsen, M. Pedersen, and J. T. Butcher, "Extracting physiological information in experimental biology via Eulerian video magnification," *BMC Biol.*, vol. 17, no. 1, pp. 1–16, 2019, doi: 10.1186/s12915-019-0716-7.

[9] H. Shahadi, Z. J. Al-Allaq, and H. Albattat, "Developed approach for phase-based Eulerian video magnification," *TELKOMNIKA*, vol. 18, no. 5, pp. 2391–2400, 2020, doi: 10.12928/telkomnika.v18i5.14321.

[10] T. Coppetti, A. Brauchlin, S. Müggler, A. Attinger-Toller, P. Biaggi, and C. A. Wyss, "Accuracy of smartphone apps for heart rate measurement," *Eur. J. Prev. Cardiol*., vol. 24, no. 12, pp. 1287–1293, 2017, doi: 10.1177/2047487317702044.

[11] R. Zhao, L. Du, Z. Zhao, X. Chen, J. Sun, Z. Man, B. Cao, and Z. Fang, "Accurate estimation of heart and respiration rates based on an optical fiber sensor using adaptive regulations and statistical classifications spectrum analysis," *Front. Digit. Health*, vol. 3, no. Dec., pp. 1–14, 2021, doi: 10.3389/fdgth.2021.747460.

[12] E. Gambi, A. Agostinelli, A. Belli, L. Burattini, E. Cippitelli, S. Fioretti, P. Pierleoni, M. Ricciuti, A. Sbrollini, and S. Spinsante, "Heart rate detection using Microsoft Kinect: validation and comparison to wearable devices," *Sensors*, vol. 17, no. 8, pp. 1–12, 2017, doi: 10.3390/s17081776.

[13] D. Kolosov, V. Kelefouras, P. Kourtessis, and I. Mporas, "Contactless camera-based heart rate and respiratory rate monitoring using AI on hardware," *Sensors*, vol. 23, no. 9, pp. 1–12, 2023, doi: 10.3390/s23094550.

[14] J. Ryu, S. Hong, S. Liang, S. Pak, L. Zhang, and Y. Lian, "A real-time heart rate estimation framework based on facial video while wearing a mask," *Technol. Health Care*, vol. 31, no. 3, pp. 1047–1062, 2023, doi: 10.3233/THC-220322.

[15] L. Liu, D. Yu, H. Lu, C. Shan, and W. Wang, "Camera-based seismocardiogram for heart rate variability monitoring," IEEE *J. Biomed. Health Inform*., vol. 28, no. 5, pp. 2794–2805, 2024, doi: 10.1109/JBHI.2024.3370394.

[16] Z. Hasan, S. R. Ramamurthy, and N. Roy, "CamSense: a camera-based contact-less heart activity monitoring," *Smart Health*, vol. 23, no. Jan., pp. 1–10, 2022, doi: 10.1016/j.smhl.2021.100240.

[17] M. Alnaggar, A. I. Siam, M. Handosa, T. Medhat, and M. Z. Rashad, "Video-based real-time monitoring for heart rate and respiration rate," *Expert Syst. Appl*., vol. 225, no. Jan., pp. 1–12, 2023, doi: 10.1016/j.eswa.2023.120135.

[18] F. M. Talaat, "Revolutionizing cardiovascular health: integrating deep learning techniques for predictive analysis of personal key indicators in heart disease," *Neural Comput. Appl*., vol. 37, no. 1, pp. 1–24, 2024, doi: 10.1007/s00521-024-10453-2.

[19] S. K. S. Srusti, M. P. Trupthi, S. Smitha, and N. R. Meghana, "Heart rate monitoring system using finger tip through Arduino and Processing software," *Int. J. Eng. Res. Technol*., vol. 6, no. 13, pp. 1–10, 2018, doi: 10.17577/IJERTCONV6IS13103.

[20] P. G. Pansare and M. P. Dale, "Heart rate measurement from face and wrist video," *IEEE Access*, vol. 2018, no. Dec., pp. 1–10, 2018, doi: 10.1109/ICCUBEA.2018.8697722.

[21] A. Caroppo and A. Manni and G. Rescio, "Vital signs estimation in elderly using camera-based photoplethysmography," *Multimed. Tools Appl*., vol. 83, no. Jan., pp. 65363–65386, 2024, doi: 10.1007/s11042-023-18053-3.

[22] U. Debnath and S. Kim, "A comprehensive review of heart rate measurement using remote photoplethysmography and deep learning," *Biomed. Eng. Online*, vol. 24, no. 73, pp. 1–15, 2025, doi: 10.1186/s12938-025-01405-5.

[23] Q. Chen, Y. Wang, and X. Liu, "Camera-based heart rate estimation for hospitalized newborns in the presence of motion artifacts," *Biomed. Eng. Online*, vol. 20, no. Jan., pp. 1–12, 2021, doi: 10.1186/s12938-021-00958-5.

[24] S. McDuff, S. Gontarek, and R. Picard, "Improvements in remote cardiopulmonary measurement using a five band digital camera," *IEEE Trans. Biomed. Eng*., vol. 61, no. 10, pp. 2593–2601, 2014, doi: 10.1109/TBME.2014.2323699.

[25] H. Xiao, T. Liu, Y. Sun, Y. Li, S. Zhao, and A. Avolio, "Remote photoplethysmography for heart rate measurement: a review," *Biomed. Signal Process. Control*, vol. 88, no. Jan., pp. 1–12, 2024, doi: 10.1016/j.bspc.2023.105608.

[26] A. K. Maity, J. Wang, A. Sabharwal, and S. K. Nayar, "RobustPPG: camera-based robust heart rate estimation using motion cancellation," *Biomed. Opt. Express*, vol. 13, no. 10, pp. 5447–5467, 2022, doi: 10.1364/BOE.465143.

ISSN 2723-6471

[27] A. Tohma, M. Nishikawa, T. Hashimoto, Y. Yamazaki, and G. Sun, "Evaluation of remote photoplethysmography measurement conditions toward telemedicine applications," *Sensors*, vol. 21, no. 24, pp. 1–12, 2021, doi: 10.3390/s21248357.

[28] R. Zhao, L. Du, Z. Zhao, X. Chen, J. Sun, Z. Man, B. Cao, and Z. Fang, "Accurate estimation of heart and respiration rates based on an optical fiber sensor using adaptive regulations and statistical classifications spectrum analysis," *Front. Digit. Health*, vol. 3, no. Dec., pp. 1–14, 2021, doi: 10.3389/fdgth.2021.747460.